Available online at www.sciencedirect.com
SCIENCE DIRECT®
International Journal of Solids and Structures 43 (2006) 112–131
INTERNATIONAL JOURNAL OF SOLIDS and STRUCTURES
www.elsevier.com/locate/ijsolstr

Numerical and analytical methods for in-plane dynamic response of annular disk

C.G. Koh *, P.P. Sze, T.T. Deng

Department of Civil Engineering, National University of Singapore, 10 Kent Ridge Crescent, Singapore 119260, Singapore

Received 14 August 2004; received in revised form 18 May 2005
Available online 11 July 2005

Abstract

A new method called the moving element method is formulated to solve two problems in a unified framework: (a) rotating disk subjected to stationary load and (b) stationary disk subjected to rotating load. The method involves discretization of the disk into "moving elements". But unlike in the conventional finite element method, these elements rotate relative to the disk and are not attached to material points. Analytical solutions in terms of complex Fourier–Hankel series are also presented. Numerical examples show good agreement between the proposed numerical method and the analytical method. The advantages of the proposed method over the analytical method and the finite element method are illustrated.

Keywords: Moving element method; Finite element method; Dynamics; Rotating disk

1. Introduction

Dynamic analysis of rotating (spinning) disks and circular objects alike is an important subject for many engineering applications, such as wheels, disc-brakes, disk drives and circular saw blades. These problems involve moving load problems of either a stationary disk under rotating load (SD-RL) or a rotating disk under stationary load (RD-SL). Analytical solutions are available for special circumstances and typically involve the concept of stress function. Srinivasan and Ramamurti (1979) first presented a static analysis of an annular disk with a clamped inner boundary and a concentrated, in-plane load at the outer boundary. They later studied the dynamic response of stationary annular disk to a moving

* Corresponding author. Tel.: +65 68742163; fax: +65 67791635.
E-mail address: cgkoh@nus.edu.sg (C.G. Koh).

0020-7683/$ - see front matter © 2005 Elsevier Ltd. All rights reserved.
doi:10.1016/j.ijsolstr.2005.05.013

concentrated, in-plane edge load (Srinivasan and Ramamurti, 1980). By using Lame potentials, the frequencies of free in-plane vibration for various ratios of outer–inner radii were evaluated. The steady state dynamic stresses induced by a moving concentrated load at constant angular velocity at the outer boundary were then evaluated through a Galilean transformation. This solution differed from the dynamic analysis of rotating disk subjected to stationary force in terms of the centrifugal forces and the Coriolis effect. For a special case of freely spinning disks, solutions for stress and displacement can be found in Timoshenko and Goodier (1982).

Chen and Jhu (1997) applied Fourier–Bessel series in obtaining in-plane stress and displacement distributions in a rotating annular disk under stationary edge loads. They also observed the stress and displacement behavior approaching critical velocities. This approach, with modification, is used herein to obtain analytical solution of rotating disk under stationary load. While the analytical solutions have been developed, the use of finite element method (FEM) in solving moving load problems has not been as popular. Ougang et al. (2003) pointed out that the use of FEM requires very small time steps, which results in large amount of computation. Thus, analytical solution in terms of Bessel functions was chosen over the FEM in their study of disc-brake problems.

Traditional moving load problems are typically one dimensional (1-D), for instance in the case of moving load (or train car) on rail. Such problems are typically solved by FEM. Olsson (1991) demonstrated the use of FEM to a fundamental 1-D moving load problem. This dynamic solution of a simply supported beam subjected to a constant force moving at a constant velocity by FEM was achieved by running the computation over numerous time steps. Nevertheless, as the load moves along the object, keeping track of the load location and updating of the load vector become a cumbersome necessity. Furthermore, the infinite domain (rail) has to be truncated in the FE model. It is only a matter of time that the load would be out of the truncated model rendering the solution invalid. Thus the FE model tends to be very large and only the solution away from the boundary is valid. To this end, Koh et al. (2003) proposed a new method called the moving element method (MEM) and showed its advantages over the FEM in solving 1-D moving load problems. The fundamental idea behind the MEM is that moving elements are conceptual elements which "flow" in the solid object (rail) rather than physical elements attached to the object. The idea can similarly be applied to solve the rotating disk problems as presented herein.

The proposed MEM is not the same as the moving finite element (MFE) method proposed by Keith and Robert (1981). The latter method is in fact the FEM with re-meshing by adjusting nodes to deal with critical (e.g. stress concentration) region which may move as the solution develops. On the other hand, the proposed MEM in this paper deals with conceptual *elements* in solving moving load problems and is not a method of re-meshing.

In studying the RD-SL problem, the circular disk can be seen as an infinite domain along the azimuth direction. The disk is assumed to rotate at a constant angular velocity Ω anticlockwise. The disk thickness is small compared to the radius, and the disk is assumed to be in a plane stress state under in-plane forces only. The problem is thus two-dimensional (2-D) and uniform line loads across the thickness appear as point loads. The analytical solutions in terms of Fourier–Bessel series are available as mentioned earlier, by Chen and Jhu (1997). Nevertheless, the analytical solutions can be made more compact by solving the differential equations in the *complex* domain by means of complex Fourier and Hankel functions. This will be presented in the section on analytical method in this paper.

The annular disk is clamped to a rigid shaft at the inner boundary (radius $r = r_i$) and subjected to some in-plane forces at the otherwise stress-free outer radius ($r = r_o$). The disk is of constant thickness h. F_N and F_T denote, respectively, normal point force and tangential point force (per unit thickness). But they can also be distributed, or patch, loads. The applied forces are constant in magnitude and the steady state response is to be obtained. Material is assumed to be homogeneous and isotropic with Young's modulus E, Poisson's ratio v and density ρ.

2. Moving element method

The proposed MEM can be seen as a variation of the conventional finite element method. The main difference lies in the fact that moving elements are *not* attached to material points of the solid model. The coordinate transformation technique has been applied by several authors in the past to relate the rotating and referential coordinate systems (e.g. Oden and Lin, 1986). To the authors' knowledge, none has offered interpretation of various terms associated with the rotating coordinate transformation, which this paper attempts to address. And the coordinate transformation technique in the FEM has only been applied to moving object problem. The MEM proposed herein is capable of handling general problems of relative motion, including rotating load on fixed object and fixed load on rotating object. In the RD-SL case shown in Fig. 1, the elements used in the MEM remain stationary in the physical space but the rotating disk "flows" through the elements. Two coordinate systems are needed: a load-reference coordinate system (r,η) where η is the circumferential coordinate referenced to the stationary load and a disk-reference coordinate system (r,θ) where θ is the circumferential coordinate attached to the rotating disk. In the SD-RL case shown in Fig. 1, the elements used in the MEM rotate at the same velocity as the rotating force while the disk is stationary. Again the two coordinate systems are used: a load-reference coordinate system (r,η) where η rotates with the load and a disk-reference coordinate system (r,θ) where θ is referenced to the stationary disk. In either case, the elements move relative to the physical object (disk). Moving elements are thus conceptual elements rather than physical elements, and the material points of the disk may be seen as "flowing" through these elements. As a result, the applied force always acts at the same elements and nodes. In contrast, since the elements used in the FEM are attached to the disk, there is a cumbersome need of keeping track where the force is applied and updating the load vector. There is a limitation in the MEM, however,

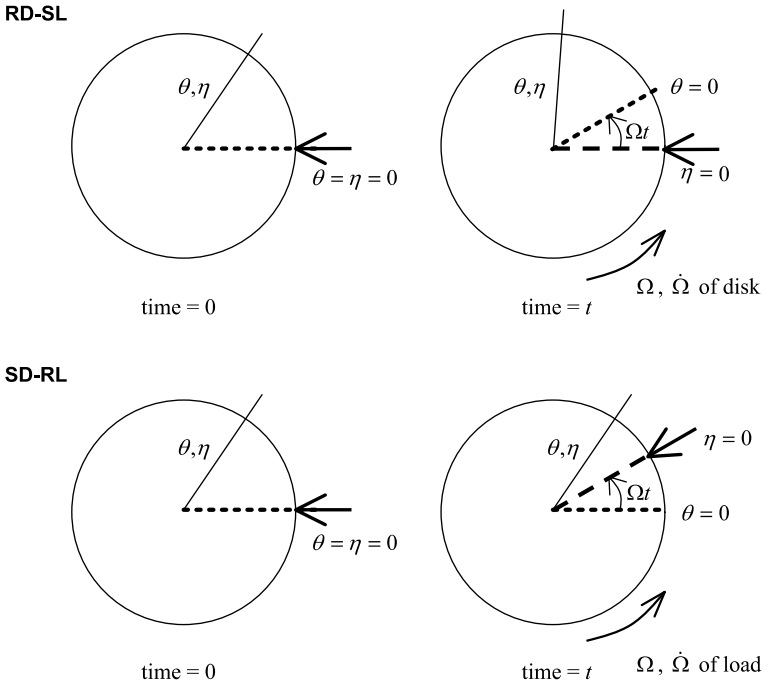

Fig. 1. Problems of RD-SL and SD-RL.

that the material domain must be identical in the direction of moving elements. In the context of this study, this implies that the disk has to be axisymmetric.

The domain of the annular disk is discretized into a number of moving elements, by "bands" in the radial direction and "sectors" in the azimuth direction. An example is illustrated in Fig. 2(a) for 5 bands and 12 sectors, and hence a total of 60 elements. Six-node elements are used in this study. Fig. 2(b) shows a typical element with two straight sides in the radial direction and two circular arc sides in the azimuth direction. Three nodes along each circular arc side are needed for reason that will be explained later. At each node, there are two degrees of freedom (DOFs). Let u_r and u_θ be the displacements in the radial and circumferential directions, respectively. The nodal displacements at the six nodes of the element are collected in the following nodal displacement vector.

$$\mathbf{U} = \begin{pmatrix} u_{r1} & u_{\theta 1} & u_{r2} & u_{\theta 2} & \cdots & u_{r6} & u_{\theta 6} \end{pmatrix}^{\mathrm{T}} \tag{1}$$

Displacement vector $\mathbf{u} = (u_r\ u_\theta)^{\mathrm{T}}$ at any point in the element is expressed in terms of nodal displacements by means of shape functions, as follows:

$$\mathbf{u} = \mathbf{N}\mathbf{U} \tag{2}$$

where $\mathbf{N}$ is a matrix containing the shape functions.

$$\mathbf{N} = \begin{bmatrix} N_1 & 0 & N_2 & 0 & \cdots & N_6 & 0 \\ 0 & N_1 & 0 & N_2 & \cdots & 0 & N_6 \end{bmatrix} \tag{3}$$

Note that the shape functions are necessarily defined in the (r,η) coordinate system instead of the (r,θ) coordinate system. The (r,η) coordinate system rotates *relative* to the disk and may be called the rotating coordinate system. Assuming polynomial shapes of the lowest order possible, an example of the shape functions used is

$$N_1 = \frac{2}{\Delta R \Delta \eta^2}(r - R_2)(\eta - \eta_2)(\eta - \eta_3) \tag{4}$$

where R_1 and R_2 are radii of the outer arc 1–2–3 and inner arc 4–5–6, respectively, η_1, η_2 and η_3 are the polar angles (in radian) of radial lines 1–6, 2–5 and 3–4, respectively. The band width and sectorial angle of the element are, respectively, $\Delta R = R_1 - R_2$ and $\Delta\eta = \eta_3 - \eta_1$. Accordingly, displacement within the element is assumed to be linear along radial lines and quadratic along arc lines.

Strain vector $\boldsymbol{\varepsilon} = (\varepsilon_{rr}\ \varepsilon_{\theta\theta}\ \gamma_{r\theta})^{\mathrm{T}}$ can be expressed in terms of nodal displacements as

$$\boldsymbol{\varepsilon} = \mathbf{B}\mathbf{U} \tag{5}$$

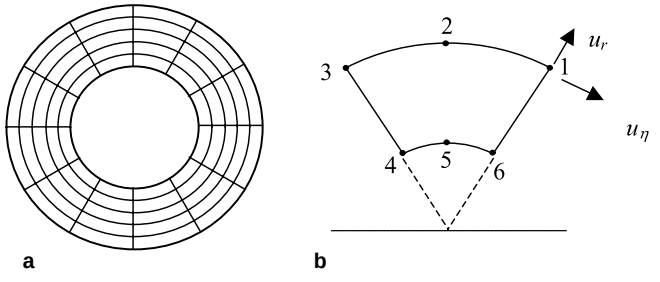

Fig. 2. (a) Mesh of 5×12 moving elements. (b) A typical element.

where

$$\mathbf{B}=\begin{bmatrix} \frac{\partial N_1}{\partial r} & 0 & \frac{\partial N_2}{\partial r} & 0 & \cdots & \frac{\partial N_6}{\partial r} & 0 \\ \frac{N_1}{r} & \frac{1}{r}\frac{\partial N_1}{\partial \eta} & \frac{N_2}{r} & \frac{1}{r}\frac{\partial N_2}{\partial \eta} & \cdots & \frac{N_6}{r} & \frac{1}{r}\frac{\partial N_6}{\partial \eta} \\ \frac{1}{r}\frac{\partial N_1}{\partial \eta} & \frac{\partial N_1}{\partial r}-\frac{N_1}{r} & \frac{1}{r}\frac{\partial N_2}{\partial \eta} & \frac{\partial N_2}{\partial r}-\frac{N_2}{r} & \cdots & \frac{1}{r}\frac{\partial N_6}{\partial \eta} & \frac{\partial N_6}{\partial r}-\frac{N_6}{r} \end{bmatrix} \tag{6}$$

Note again that the above is formulated in the rotating coordinate (r,η) system. The stress vector $\boldsymbol{\sigma}$ is related to the strain vector through the elasticity matrix $\mathbf{D}$.

$$\boldsymbol{\sigma}=\mathbf{D}\boldsymbol{\varepsilon} \tag{7}$$

For plane stress state,

$$\mathbf{D}=\frac{E}{1-v^2}\begin{bmatrix} 1 & v & 0 \\ v & 1 & 0 \\ 0 & 0 & \frac{1-v}{2} \end{bmatrix} \tag{8}$$

Substituting Eq. (5) into Eq. (7) gives

$$\boldsymbol{\sigma}=\mathbf{DBU} \tag{9}$$

The virtual displacement method is applied. Adopting a consistent formulation, the same set of shape functions is used in the virtual system (denoted by over bar). Thus,

$$\overline{\mathbf{u}}=\mathbf{N}\overline{\mathbf{U}} \tag{10}$$

$$\overline{\boldsymbol{\varepsilon}}=\mathbf{B}\overline{\mathbf{U}} \tag{11}$$

The internal virtual work is given by the following integral over the element considered.

$$W_{\mathrm{I}}=\int_{\mathrm{Element}}\overline{\boldsymbol{\varepsilon}}^{\mathrm{T}}\boldsymbol{\sigma}\,\mathrm{d}V \tag{12}$$

Using Eqs. (9) and (11) and expressing in the (r,θ) coordinate system, it can be shown that

$$W_{\mathrm{I}}=\overline{\mathbf{U}}^{\mathrm{T}}\left\{\int\int\mathbf{B}^{\mathrm{T}}\mathbf{DB}hr\,\mathrm{d}r\,\mathrm{d}\theta\right\}\mathbf{U} \tag{13}$$

The external virtual work involves nodal forces and inertial forces. The former is represented by a nodal force vector $\mathbf{F}$, whereas the latter requires acceleration at every material point in the element. Accordingly, the external virtual work is given by

$$W_{\mathrm{E}}=\overline{\mathbf{U}}^{\mathrm{T}}\mathbf{F}-\overline{\mathbf{U}}^{\mathrm{T}}\int\int\mathbf{N}^{\mathrm{T}}\rho\mathbf{a}hr\,\mathrm{d}r\,\mathrm{d}\theta \tag{14}$$

where $\mathbf{a}=(a_r\ \ a_\theta)^{\mathrm{T}}$ is the acceleration vector defined in the fixed coordinate system (r,θ). The difference between the RD-SL problem and SD-RL problem lies mainly in the derivation of acceleration vectors. As will be shown later, the SD-RL formulation can be treated as a special case of the RD-SL formulation; hence a unified framework for both problems is presented.

2.1. RD-SL problem

Consider the following position vector for a material point

$$\mathbf{r}=(r+u_r)\mathbf{e}_r+u_\theta\mathbf{e}_\theta \tag{15}$$

Velocity vector ($\mathbf{v}$) and acceleration vector ($\mathbf{a}$) are obtained as follows

$$\mathbf{v} = \frac{\mathrm{d}\mathbf{r}}{\mathrm{d}t} = (\dot{r} + \dot{u}_r - u_\theta\dot{\theta})\mathbf{e}_r + (r\dot{\theta} + u_r\dot{\theta} + \dot{u}_\theta)\mathbf{e}_\theta \tag{16}$$

$$\mathbf{a} = \frac{\mathrm{d}\mathbf{v}}{\mathrm{d}t} = \left(\ddot{r} + \ddot{u}_r - 2\dot{u}_\theta\dot{\theta} - u_\theta\ddot{\theta} - (r+u_r)\dot{\theta}^2\right)\mathbf{e}_r + (2\dot{r}\dot{\theta} + 2\dot{u}_r\dot{\theta} - u_\theta\dot{\theta}^2 + r\ddot{\theta} + u_r\ddot{\theta} + \ddot{u}_\theta)\mathbf{e}_\theta \tag{17}$$

where $\dot{r} = \ddot{r} = 0$, $\dot{\theta} = \Omega$, $\ddot{\theta} = 0$ at steady state. Hence

$$\mathbf{a} = \ddot{\mathbf{u}} + 2\Omega\begin{bmatrix} -\dot{u}_\theta \\ \dot{u}_r \end{bmatrix} + r\Omega^2\begin{bmatrix} -1 \\ 0 \end{bmatrix} - \Omega^2\begin{bmatrix} u_r \\ u_\theta \end{bmatrix} \tag{18}$$

The right-hand-side of the above equation contains acceleration relative to the rotating frame (first term), the Coriolis acceleration (second term) and centrifugal forces (third and fourth terms). By applying the following coordinate transformation

$$\eta = \theta + \Omega t \tag{19}$$

it can be derived that

$$\frac{\mathrm{d}\mathbf{u}(r,\theta)}{\mathrm{d}t} = \Omega\frac{\partial\mathbf{u}(r,\eta)}{\partial\eta} + \frac{\partial\mathbf{u}(r,\eta)}{\partial t} \tag{20a}$$

$$\frac{\mathrm{d}^2\mathbf{u}(r,\theta)}{\mathrm{d}t^2} = \frac{\partial^2\mathbf{u}(r,\eta)}{\partial t^2} + 2\Omega\frac{\partial^2\mathbf{u}(r,\eta)}{\partial t\partial\eta} + \Omega^2\frac{\partial^2\mathbf{u}(r,\eta)}{\partial\eta^2} \tag{20b}$$

Making use of shape functions as defined in Eq. (4), these equations can be written as

$$\frac{\mathrm{d}\mathbf{u}(r,\theta)}{\mathrm{d}t} = \Omega\mathbf{u}_{,\eta} + \dot{\mathbf{u}} = \Omega\mathbf{N}_{,\eta}\mathbf{U} + \mathbf{N}\dot{\mathbf{U}} \tag{21a}$$

$$\frac{\mathrm{d}^2\mathbf{u}(r,\theta)}{\mathrm{d}t^2} = \ddot{\mathbf{u}} + 2\Omega\dot{\mathbf{u}}_{,\eta} + \Omega^2\mathbf{u}_{,\eta\eta} = \mathbf{N}\ddot{\mathbf{U}} + 2\Omega\mathbf{N}_{,\eta}\dot{\mathbf{U}} + \Omega^2\mathbf{N}_{,\eta\eta}\mathbf{U} \tag{21b}$$

The above equations involve partial derivatives of shape functions with respect to η, i.e. $\mathbf{N}_{,\eta}$ and $\mathbf{N}_{,\eta\eta}$. This explains why the polynomial shape functions have to be of at least second order in η; hence a minimum of three nodes along the azimuth direction for the element.

For the Coriolis acceleration term in Eq. (18), it is convenient to introduce the following shape function matrix for ease of formulation.

$$\hat{\mathbf{N}} = \begin{bmatrix} 0 & -N_1 & 0 & -N_2 & \cdots & 0 & -N_6 \\ N_1 & 0 & N_2 & 0 & \cdots & N_6 & 0 \end{bmatrix} \tag{22}$$

Thus,

$$\begin{bmatrix} -u_\theta \\ u_r \end{bmatrix} = \hat{\mathbf{N}}\mathbf{U} \tag{23a}$$

$$\begin{bmatrix} -\dot{u}_\theta \\ \dot{u}_r \end{bmatrix} = \Omega\hat{\mathbf{N}}_{,\eta}\mathbf{U} + \hat{\mathbf{N}}\dot{\mathbf{U}} \tag{23b}$$

Eq. (18) can now be written as

$$\mathbf{a} = \mathbf{N}\ddot{\mathbf{U}} + 2\Omega\mathbf{N}_{,\eta}\dot{\mathbf{U}} + \Omega^2\mathbf{N}_{,\eta\eta}\mathbf{U} + 2\Omega^2\hat{\mathbf{N}}_{,\eta}\mathbf{U} + 2\Omega\hat{\mathbf{N}}\dot{\mathbf{U}} + r\Omega^2\begin{bmatrix} -1 \\ 0 \end{bmatrix} - \Omega^2\mathbf{N}\mathbf{U} \tag{24}$$

Equating W_E and W_I, using the above equation and expressing the integral in the (r,η) coordinate system yield the following equations of motion

$$\mathbf{MA} + \mathbf{CV} + \mathbf{KU} = \mathbf{P}(t) \tag{25}$$

where the equivalent mass, damping and stiffness matrices for the element are, respectively,

$$\mathbf{M} = \int\int \mathbf{N}^{\mathrm{T}} \rho \mathbf{N} h r \,\mathrm{d}r \,\mathrm{d}\eta \tag{26a}$$

$$\mathbf{C} = 2\Omega \int\int \mathbf{N}^{\mathrm{T}} \rho \mathbf{N}_{,\eta} h r \,\mathrm{d}r \,\mathrm{d}\eta + 2\Omega \int\int \mathbf{N}^{\mathrm{T}} \rho \hat{\mathbf{N}} h r \,\mathrm{d}r \,\mathrm{d}\eta \tag{26b}$$

$$\mathbf{K} = \int\int \mathbf{B}^{\mathrm{T}} \mathbf{D} \mathbf{B} h r \,\mathrm{d}r \,\mathrm{d}\theta + \Omega^2 \int\int \mathbf{N}^{\mathrm{T}} \rho \mathbf{N}_{,\eta\eta} h r \,\mathrm{d}r \,\mathrm{d}\eta + 2\Omega^2 \int\int \mathbf{N}^{\mathrm{T}} \rho \hat{\mathbf{N}}_{,\eta} h r \,\mathrm{d}r \,\mathrm{d}\eta - \Omega^2 \int\int \mathbf{N}^{T} \rho \mathbf{N} h r \,\mathrm{d}r \,\mathrm{d}\eta \tag{26c}$$

and the equivalent load vector is

$$\mathbf{P}(t) = \mathbf{F}(t) - \int\int \mathbf{N}^{\mathrm{T}} \rho r \Omega^2 \begin{bmatrix} -1 \\ 0 \end{bmatrix} h r \,\mathrm{d}r \,\mathrm{d}\eta \tag{27}$$

where $\mathbf{F}$ is the external applied load vector to the rotating disk. By the direct stiffness method, the element matrices and the load vector are assembled to form the corresponding structure matrices and vector, leading to

$$\mathbf{M}_{\mathrm{s}}\mathbf{A}_{\mathrm{s}} + \mathbf{C}_{\mathrm{s}}\mathbf{V}_{\mathrm{s}} + \mathbf{K}_{\mathrm{s}}\mathbf{U}_{\mathrm{s}} = \mathbf{P}_{\mathrm{s}}(t) \tag{28}$$

where subscript s denotes the structure (disk).

In the present study, the applied load is constant and thus $\mathbf{P}_{\mathrm{s}}$ is not a function of time. At steady state with the disk rotating at a constant angular velocity Ω, Eq. (27) in fact reduces to an equivalent static system which can be solved much more efficiently than dynamic equations.

$$\mathbf{K}_{\mathrm{s}}\mathbf{U}_{\mathrm{s}} = \mathbf{P}_{\mathrm{s}} \tag{29}$$

2.2. SD-RL problem

Based on the above formulation for solving the RD-SL problem, the SD-RL problem can in fact be solved as a special case with minor changes. In contrast to Eq. (18), since the disk is stationary, the acceleration (of material particle) is simply given by

$$\mathbf{a} = \frac{\mathrm{d}^2\mathbf{u}(r,\theta)}{\mathrm{d}t^2} \tag{30}$$

Applying coordinate transformation leads to

$$\mathbf{a} = \ddot{\mathbf{u}} + 2\Omega\mathbf{N}_{,\eta}\dot{\mathbf{u}} + \Omega^2\mathbf{u}_{,\eta\eta} = \mathbf{N}\ddot{\mathbf{U}} - 2\Omega\mathbf{N}_{,\eta}\dot{\mathbf{U}} + \Omega^2\mathbf{N}_{,\eta\eta}\mathbf{U} \tag{31}$$

In view of the above, it can be shown that the equivalent mass matrix remains the same as in Eq. (26a) whereas the equivalent damping and stiffness matrices are

$$\mathbf{C} = 2\Omega \int\int \mathbf{N}^{\mathrm{T}} \rho \mathbf{N}_{,\eta} h r \,\mathrm{d}r \,\mathrm{d}\eta \tag{32a}$$

$$\mathbf{K} = \int\int \mathbf{B}^{\mathrm{T}} \mathbf{D} \mathbf{B} h r \,\mathrm{d}r \,\mathrm{d}\theta + \Omega^2 \int\int \mathbf{N}^{\mathrm{T}} \rho \mathbf{N}_{,\eta\eta} h r \,\mathrm{d}r \,\mathrm{d}\eta \tag{32b}$$

Hence, the formulation for the SD-RL case can be treated as a special case in the RD-SL solution procedure by simply suppressing the terms associated with Coriolis and centrifugal effects.

3. Analytical method

Analytical solution in terms of complex Fourier–Hankel is formulated for comparison with the MEM solution. The governing equations can be expressed in respect to the disk-reference coordinate as

$$\frac{E}{\rho(1-v^2)}(L_{11}u_r + L_{12}u_\theta) = \ddot{u}_r - 2\Omega\dot{u}_\theta - \Omega^2(u_r + r) \tag{33a}$$

$$\frac{E}{\rho(1-v^2)}(L_{21}u_r + L_{22}u_\theta) = \ddot{u}_\theta + 2\Omega\dot{u}_r - \Omega^2 u_\theta \tag{33b}$$

where the differential operators are defined as (Chen and Jhu, 1997)

$$L_{11} = \frac{\partial^2}{\partial r^2} + \frac{1}{r}\frac{\partial}{\partial r} - \frac{1}{r^2} + \frac{1-v}{2r^2}\frac{\partial^2}{\partial\theta^2} \tag{34a}$$

$$L_{12} = \frac{1+v}{2}\frac{1}{r}\frac{\partial^2}{\partial r\partial\theta} - \frac{3-v}{2}\frac{1}{r^2}\frac{\partial}{\partial\theta} \tag{34b}$$

$$L_{21} = \frac{1+v}{2}\frac{1}{r}\frac{\partial^2}{\partial r\partial\theta} + \frac{3-v}{2}\frac{1}{r^2}\frac{\partial}{\partial\theta} \tag{34c}$$

$$L_{22} = \frac{1-v}{2}\left(\frac{\partial^2}{\partial r^2} + \frac{1}{r}\frac{\partial}{\partial r} - \frac{1}{r^2}\right) + \frac{1}{r^2}\frac{\partial^2}{\partial\theta^2} \tag{34d}$$

Using the same transformation as Eq. (19), the following equations can be derived

$$\dot{u}_r(r,\theta) = \frac{\partial u_r(r,\eta)}{\partial t} + \Omega\frac{\partial u_r(r,\eta)}{\partial\eta} \tag{35a}$$

$$\ddot{u}_r(r,\theta) = \frac{\partial^2 u_r(r,\eta)}{\partial t^2} + 2\Omega\frac{\partial^2 u_r(r,\eta)}{\partial t\partial\eta} + \Omega^2\frac{\partial^2 u_r(r,\eta)}{\partial\eta^2} \tag{35b}$$

Following the solution procedure by Chen and Jhu (1997), this case can be separated into two sub-problems: (1) inhomogeneous equations with homogeneous boundary conditions and (2) homogeneous equations with inhomogeneous boundary conditions.

To facilitate the analytical solution, it is necessary to assume that u_r is small and negligible when compared to r. Thus the term $u_r\Omega^2$ in Eq. (33a) is ignored in the analytical solution (but not in the MEM solution presented earlier). The first sub-problem is thus the same as the classical problem of freely spinning disk (Timoshenko and Goodier, 1982).

For the second sub-problem, the following dimensionless variables are introduced and denoted with overhead bars:

$$\bar{r} = \frac{r}{r_o}, \quad \bar{\xi} = \frac{r_i}{r_o}, \quad \bar{u}_r = \frac{u_r}{r_o}, \quad \bar{u}_\eta = \frac{u_\eta}{r_o}, \quad \bar{\Omega} = \Omega r_o\sqrt{\frac{\rho}{E}}, \quad \bar{t} = \frac{t}{r_o}\sqrt{\frac{E}{\rho}} \quad \bar{\sigma}_{rr} = \frac{\sigma_{rr}}{E},$$

$$\bar{\sigma}_{\eta\eta} = \frac{\sigma_{\eta\eta}}{E}, \quad \bar{\tau}_{r\eta} = \frac{\tau_{r\eta}}{E}$$

For brevity, however, the overhead bars are ignored from here onwards. By using Lame's potential ϕ and ψ, the displacement can be expressed as

$$u_r = \frac{\partial \phi}{\partial r} + \frac{1}{r}\frac{\partial \psi}{\partial \eta} \tag{36a}$$

$$u_\eta = \frac{1}{r}\frac{\partial \phi}{\partial \eta} - \frac{\partial \psi}{\partial r} \tag{36b}$$

Considering steady state and substituting the above equations into Eq. (33), it can be shown that

$$\frac{\partial G}{\partial r} + \frac{1}{r}\frac{\partial H}{\partial \eta} = 0 \tag{37a}$$

$$\frac{1}{r}\frac{\partial G}{\partial \eta} - \frac{\partial H}{\partial r} = 0 \tag{37b}$$

where

$$G = \zeta_1^2 \nabla^2 \phi - \Omega^2 \frac{\partial^2 \phi}{\partial \eta^2} + \Omega^2 \phi - 2\Omega^2 \frac{\partial \psi}{\partial \eta} \tag{38a}$$

$$H = \zeta_2^2 \nabla^2 \psi - \Omega^2 \frac{\partial^2 \psi}{\partial \eta^2} + \Omega^2 \psi - 2\Omega^2 \frac{\partial \phi}{\partial \eta} \tag{38b}$$

$$\zeta_1^2 = \frac{1}{1-v^2}, \quad \zeta_2^2 = \frac{1}{2(1+v)} \tag{39}$$

By solving Eq. (37) to obtain solutions for ϕ and ψ, in-plane stress and displacements for the case of rotating disk subjected to stationary *normal* load can be obtained. The solution procedure is made more compact by using complex Fourier–Hankel functions instead of real Fourier–Bessel functions given by Chen and Jhu (1997).

$$\begin{aligned} u_r = {} & \exp(\mathrm{i}\eta)\left\{\frac{A_1}{2\Omega^2} + B_1\left[\mu_1(1+2\ln r) + \frac{1}{2}\frac{\mu_2}{\mu_0}r^{-2}\right]\right\} + \sum_{n=0}^{\infty} \exp(\mathrm{i}n\eta)\{c_n[k_{n8}r^{-1}H_n^{(1)}(\beta_{n1}r) \\ & - \beta_{n1}H_{n+1}^{(1)}(\beta_{n1}r)] + d_n[k_{n7}r^{-1}H_n^{(1)}(\beta_{n2}r) - s_{n1}\beta_{n2}H_{n+1}^{(1)}(\beta_{n2}r)] + e_n[k_{n8}r^{-1}H_n^{(2)}(\beta_{n1}r) \\ & - \beta_{n1}H_{n+1}^{(2)}(\beta_{n1}r)] + f_n[k_{n7}r^{-1}H_n^{(2)}(\beta_{n2}r) - s_{n1}\beta_{n2}H_{n+1}^{(2)}(\beta_{n2}r)]\} \end{aligned} \tag{40a}$$

$$\begin{aligned} u_\eta = {} & \mathrm{i}\exp(\mathrm{i}\eta)\left\{\frac{A_1}{2\Omega^2} + B_1\left[\mu_1(1+2\ln r) - \frac{1}{2}\frac{\mu_2}{\mu_0}r^{-2}\right]\right\} + \sum_{n=0}^{\infty} -\mathrm{i}\exp(\mathrm{i}n\eta)\{c_n[s_{n2}\beta_{n1}H_{n+1}^{(1)}(\beta_{n1}r) \\ & - k_{n8}r^{-1}H_n^{(1)}(\beta_{n1}r)] + d_n[\beta_{n2}H_{n+1}^{(1)}(\beta_{n2}r) - k_{n7}r^{-1}H_n^{(1)}(\beta_{n2}r)] + e_n[s_{n2}\beta_{n1}H_{n+1}^{(2)}(\beta_{n1}r) \\ & - k_{n8}r^{-1}H_n^{(2)}(\beta_{n1}r)] + f_n[\beta_{n2}H_{n+1}^{(2)}(\beta_{n2}r) - k_{n7}r^{-1}H_n^{(2)}(\beta_{n2}r)]\} \end{aligned} \tag{40b}$$

$$\begin{aligned} (1-v^2)\sigma_{rr} = {} & B_1(2\mu_1 r^{-1} - \mu_2 r^{-3})\exp(\mathrm{i}\eta) + \sum_{n=0}^{\infty} \exp(\mathrm{i}n\eta)\{c_n[(k_{n1}r^{-2} - \beta_{n1}^2)H_n^{(1)}(\beta_{n1}r) \\ & + k_{n2}r^{-1}H_{n+1}^{(1)}(\beta_{n1}r)] + d_n[(k_{n3}r^{-2} - s_{n1}\beta_{n2}^2)H_n^{(1)}(\beta_{n2}r) + k_{n4}r^{-1}H_{n+1}^{(1)}(\beta_{n2}r)] \\ & + e_n[(k_{n1}r^{-2} - \beta_{n1}^2)H_n^{(2)}(\beta_{n1}r) + k_{n2}r^{-1}H_{n+1}^{(2)}(\beta_{n1}r)] + f_n[(k_{n3}r^{-2} - s_{n1}\beta_{n2}^2)H_n^{(2)}(\beta_{n2}r) \\ & + k_{n4}r^{-1}H_{n+1}^{(2)}(\beta_{n2}r)]\} \end{aligned} \tag{40c}$$

$$(1-\nu^2)\tau_{r\eta} = B_1(\mu_0\mu_1 r^{-1} + \mu_2 r^{-3})\mathrm{i}\exp(\mathrm{i}n\eta) + \sum_{n=0}^{\infty} -\mathrm{i}\exp(\mathrm{i}n\eta)\left\{c_n\left[\left(\frac{1}{2}\mu_0 s_{n2}\beta_{n1}^2 - k_{n1}r^{-2}\right)H_n^{(1)}(\beta_{n1}r)\right.\right.$$
$$\left. - k_{n5}r^{-1}H_{n+1}^{(1)}(\beta_{n1}r)\right] + d_n\left[\left(\frac{1}{2}\mu_0\beta_{n2}^2 - k_{n3}r^{-2}\right)H_n^{(1)}(\beta_{n1}r) - k_{n6}r^{-1}H_{n+1}^{(1)}(\beta_{n2}r)\right]$$
$$+ e_n\left[\left(\frac{1}{2}\mu_0 s_{n2}\beta_{n1}^2 - k_{n1}r^{-2}\right)H_n^{(2)}(\beta_{n1}r) - k_{n5}r^{-1}H_{n+1}^{(2)}(\beta_{n1}r)\right]$$
$$\left. + f_n\left[\left(\frac{1}{2}\mu_0\beta_{n2}^2 - k_{n3}r^{-2}\right)H_n^{(2)}(\beta_{n1}r) - k_{n6}r^{-1}H_{n+1}^{(2)}(\beta_{n2}r)\right]\right\} \tag{40d}$$

$$(1-\nu^2)\sigma_{\eta\eta} = B_1(2\nu\mu_1 r^{-1} + \mu_2 r^{-3})\exp(\mathrm{i}n\eta) + \sum_{n=0}^{\infty}\exp(\mathrm{i}n\eta)\{c_n[(-k_{n1}r^{-2} - \nu\beta_{n1}^2)H_n^{(1)}(\beta_{n1}r)$$
$$- k_{n2}r^{-1}H_{n+1}^{(1)}(\beta_{n1}r)] + d_n[(-k_{n3}r^{-2} - \nu s_{n1}\beta_{n2}^2)H_n^{(1)}(\beta_{n2}r) - k_{n4}r^{-1}H_{n+1}^{(1)}(\beta_{n2}r)]$$
$$+ e_n[(-k_{n1}r^{-2} - \nu\beta_{n1}^2)H_n^{(2)}(\beta_{n1}r) - k_{n2}r^{-1}H_{n+1}^{(2)}(\beta_{n1}r)] + f_n[(-k_{n3}r^{-2}$$
$$- \nu s_{n1}\beta_{n2}^2)H_n^{(2)}(\beta_{n2}r) - k_{n4}r^{-1}H_{n+1}^{(2)}(\beta_{n2}r)]\} \tag{40e}$$

where

$$\mu_0 = 1-\nu, \quad \mu_1 = (\zeta_1^2+\zeta_2^2)^{-1}, \quad \mu_2 = \mu_0\mu_1(\zeta_1^2-\zeta_2^2)\Omega^{-2}$$
$$k_{n1} = \mu_0(1+s_{n2})(n^2-n), \quad k_{n2} = \mu_0(1-ns_{n2})\beta_{n1}, \quad k_{n3} = \mu_0(1+s_{n1})(n^2-n)$$
$$k_{n4} = \mu_0(n-s_{n1})\beta_{n2}, \quad k_{n5} = -\mu_0(n-s_{n2})\beta_{n1}, \quad k_{n6} = \mu_0(1-ns_{n1})\beta_{n2}$$
$$k_{n7} = n(1+s_{n1}), \quad k_{n8} = n(1+s_{n2})$$
$$s_{n1} = \frac{2n\Omega^2}{(1+n^2)\Omega^2 - \zeta_1^2\beta_{n2}^2}, \quad s_{n2} = \frac{2n\Omega^2}{(1+n^2)\Omega^2 - \zeta_2^2\beta_{n1}^2} \qquad \text{for } n \neq 1$$

c_n, d_n, e_n and f_n are unknown complex coefficients while A_1 and B_1 are real coefficient for $n = 1$. The values for β_{n1} and β_{n2} are different at different n, as given below.

For $n = 0$, $\beta_{01} = \frac{\Omega}{\zeta_1}$ and $\beta_{02} = \frac{\Omega}{\zeta_2}$.

For $n = 1$, β_{11} and s_{12} vanish while $\beta_{12} = \frac{\sqrt{3-\nu}}{\zeta_2}$ and $s_{11} = -\frac{1-\nu}{2}$.

For $n \geqslant 2$, β_{n1} and β_{n2} are positive real roots of the equation

$$\zeta_1^2\zeta_2^2\beta^4 - (\zeta_1^2+\zeta_2^2)(1+n^2)\Omega^2\beta^2 + (1-n^2)^2\Omega^4 = 0 \tag{41}$$

Boundary conditions, also expressed in complex Fourier series, are imposed to solve the unknown coefficients. Consider normal force per unit thickness F_N applied at the outer boundary ($r = r_o$) at $\eta = 0$. The boundary conditions are

$$u_r(r_i,\eta) = u_\eta(r_i,\eta) = 0 \tag{42a}$$

$$\sigma_{rr}(r_o,\eta) = -\frac{F_N}{r_o}\delta(n) = -\frac{F_N}{2\pi r_o} - \frac{F_N}{\pi r_o}\sum_{n=1}^{\infty}\exp(\mathrm{i}n\eta) \quad \text{and} \quad \tau_{r\eta}(r_o,\eta) = 0 \text{ for normal point load} \tag{42b}$$

The real part of the complex solution gives the solution for rotating disk under normal point load. By multiplying the expression at the right-hand-side of Eq. (40) with $-\mathrm{i}$, the solution for rotating disk under tangential point load can be obtained. Obviously, the infinite series solution has to be truncated for

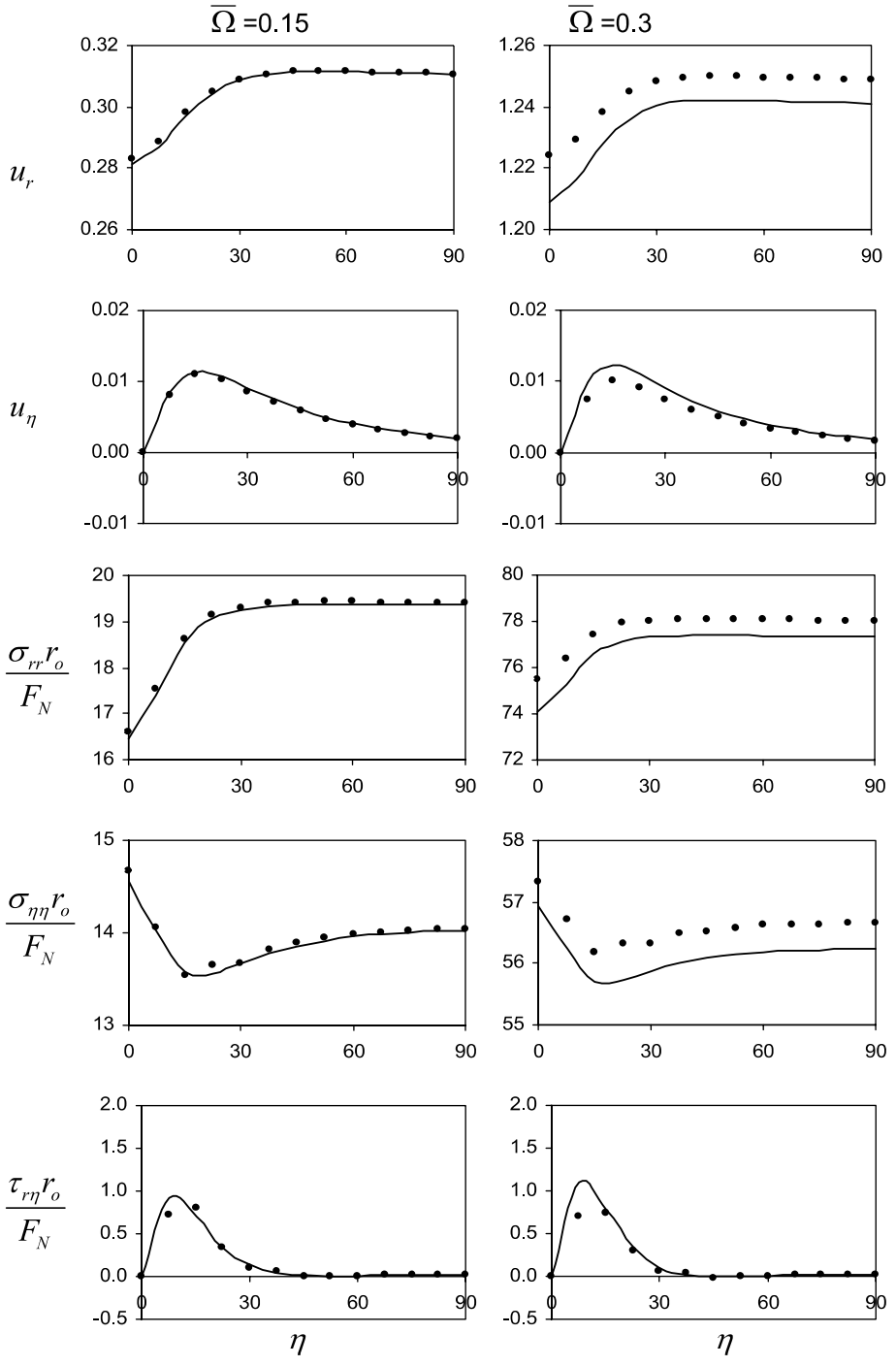

Fig. 3. Comparison of displacements and stresses along $r/r_o = 0.75$ between analytical (—) and MEM (●) solutions for a disk rotating at three different dimensionless rotating speeds, $\bar{\Omega} = 0.15$, 0.3 and subjected to normal point load.

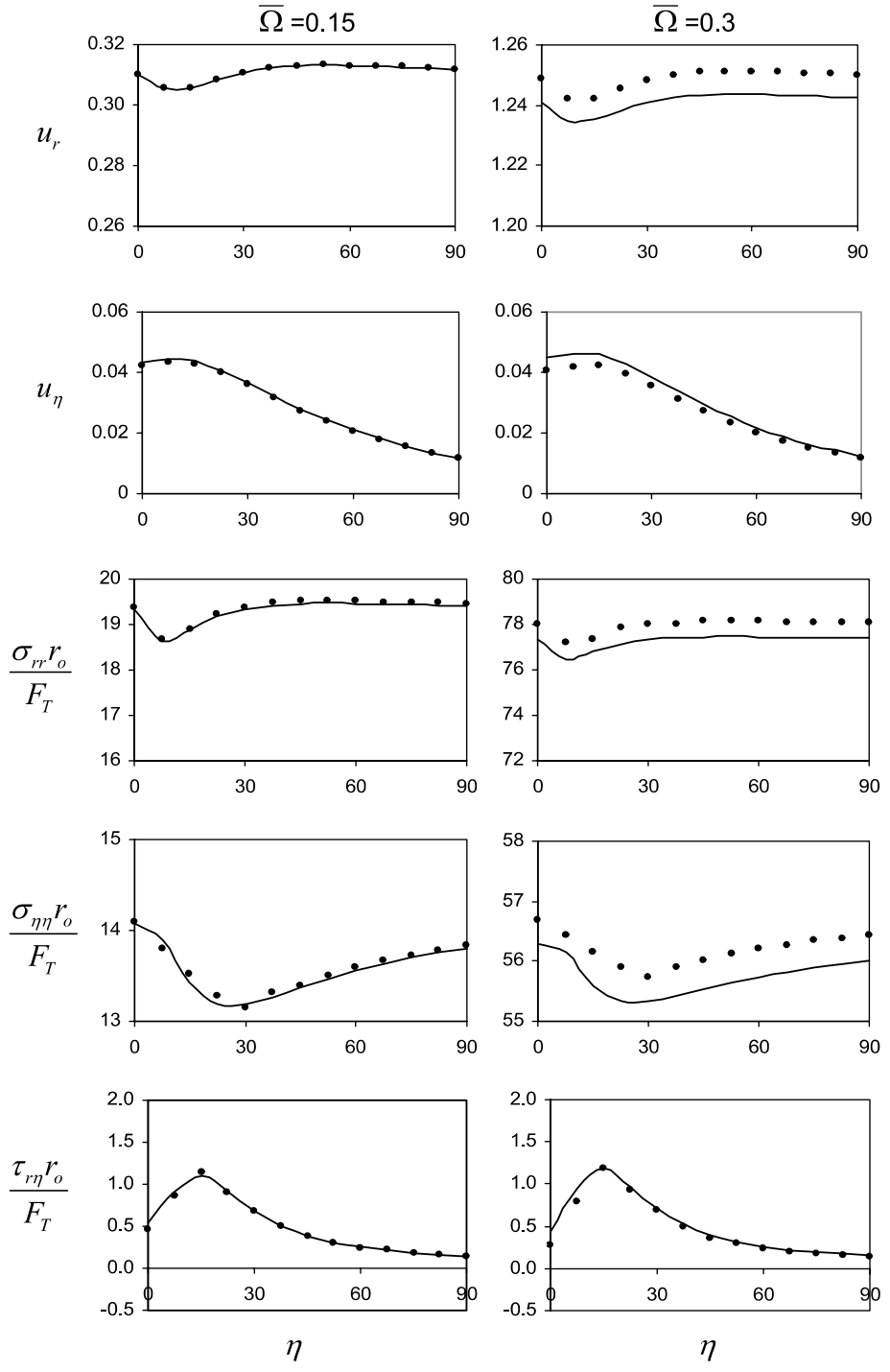

Fig. 4. Comparison of displacements and stresses along $r/r_o = 0.75$ between analytical (—) and MEM (●) solutions for a disk rotating at three different dimensionless rotating speeds, $\bar{\Omega} = 0.15$, 0.3 and subjected to tangential point load.

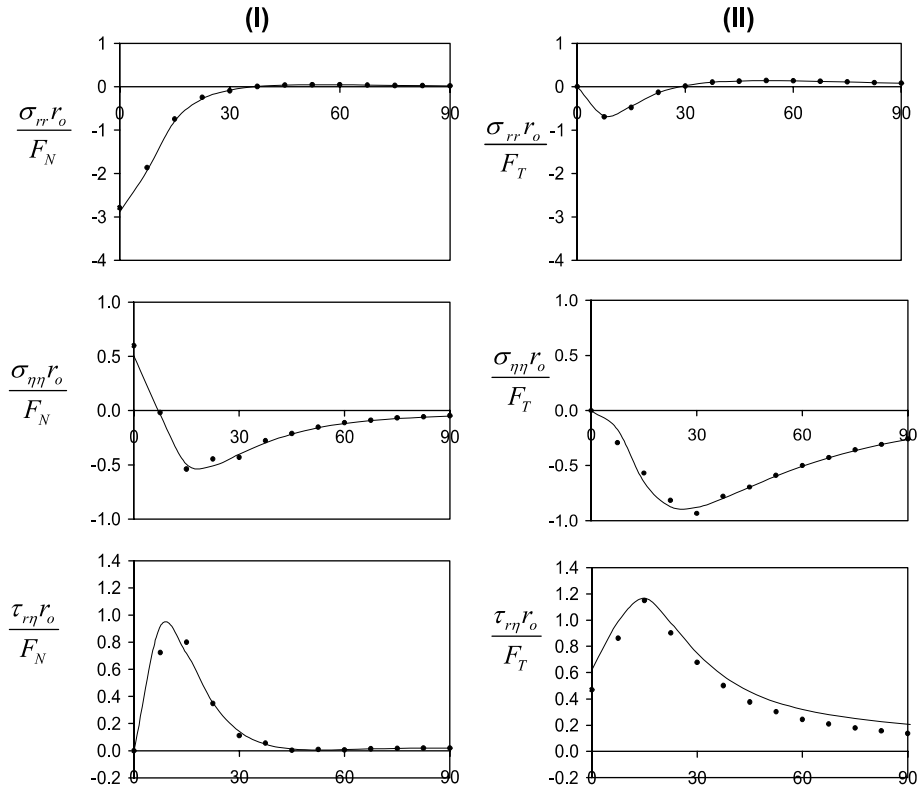

Fig. 5. Comparison of stresses along $r/r_o = 0.75$ between analytical (—) and MEM (●) solutions for a stationary disk subjected to (I) normal point load and (II) tangential point load, rotating at velocity, $\bar{\Omega} = 0.15$.

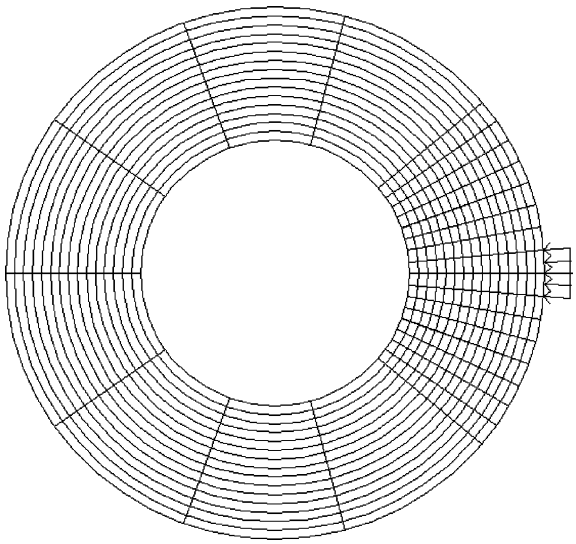

Fig. 6. A 15×24 non-uniform mesh consisting of 5° and 35° sectors.

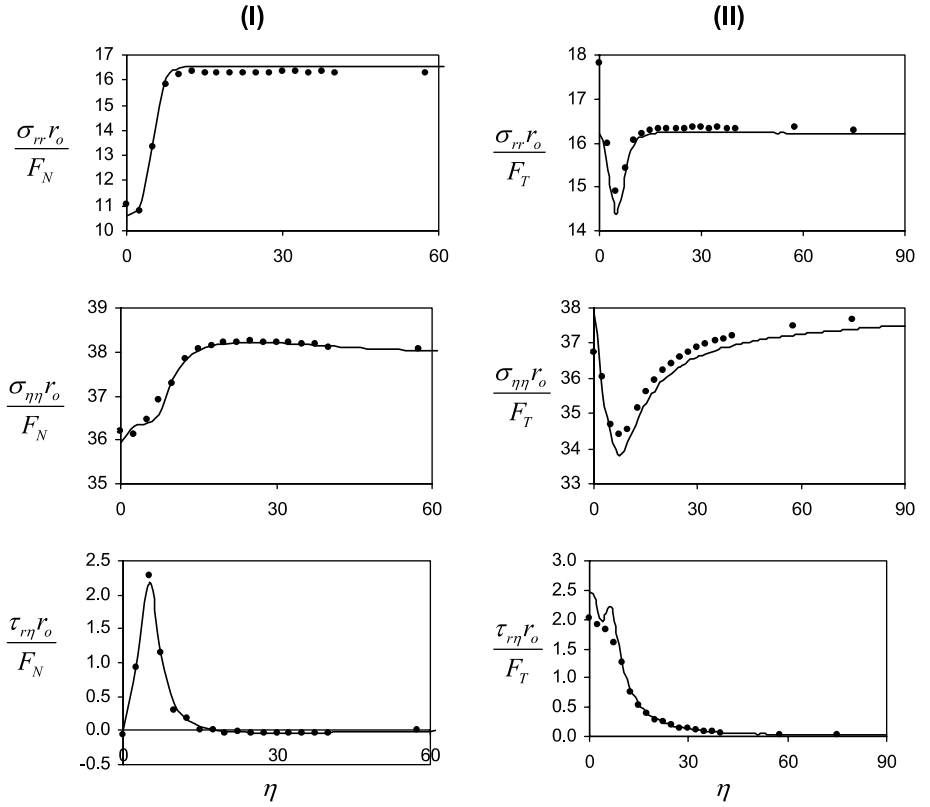

Fig. 7. Comparison of stresses along $r/r_o = 0.95$ between analytical (—) and MEM (●) solutions for a disk rotating at dimensionless rotating velocity, $\bar{\Omega} = 0.3$ and subjected to (I) normal patch load and (II) tangential patch load.

computation, resulting in a finite system of linear equations for solving the unknown coefficients. With the determined coefficients, the components of displacement and stress for various n are then superposed to obtain the actual displacement and stress at different points on the disk.

Note that point load is an idealization and the analytical solution is mathematically singular at the point of load. A more practical approach is to consider patch loading, for example, a uniformly distributed load defined as follows. Acting along the outer boundary within the angular range $-\alpha \leqslant \eta \leqslant \alpha$, the pressure can be expressed as

$$w = \frac{F}{2r_o\alpha} \tag{43}$$

Correspondingly the stress boundary conditions are

$$\sigma_{rr}(r_o, \eta) = -\frac{w_N\alpha}{\pi} - \frac{2w_N}{\pi}\sum_{n=1}^{\infty}\frac{1}{n}(\sin n\alpha)\exp(in\eta) \tag{44a}$$

$$\tau_{r\eta}(r_o, \eta) = \frac{w_T\alpha}{\pi} + \frac{2w_T}{\pi}\sum_{n=1}^{\infty}\frac{1}{n}(\sin n\alpha)\exp(in\eta) \tag{44b}$$

For the SD-RL problem, the solution given by Srinivasan and Ramamurti (1979) can be made more compact similarly by adopting complex Fourier–Hankel series, as shown in Appendix A.

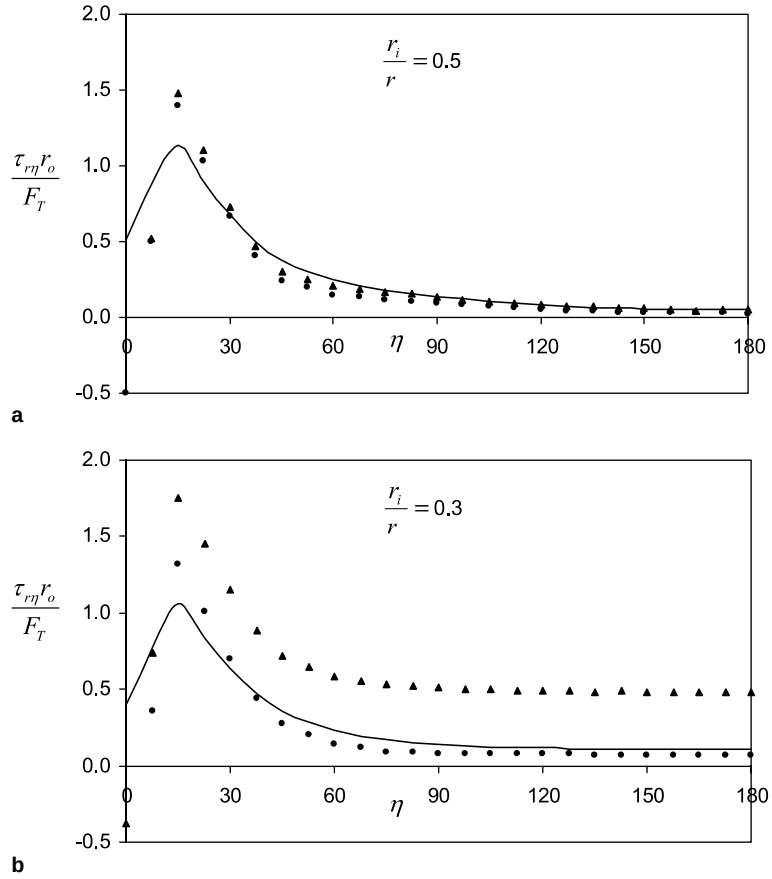

Fig. 8. Comparison of shear stresses at $r/r_o = 0.75$ for annular disk with radius ratio of (a) 0.5 and (b) 0.3 subjected to tangential point load. (—) Corresponds to stationary disk subjected to stationary load, (●) to stationary disk subjected to load rotating at $\bar{\Omega} = 0.5$ and (▲) to disk rotating at $\bar{\Omega} = 0.5$ subjected to stationary load.

4. Numerical examples and discussion

The following parameters are considered: $E = 200$ GPa, $\rho = 7860$ kg/m^3, $v = 0.3$, $r_i = 0.1$ m, $r_o = 0.2$ m, $h = 0.01$ m, F_N (or F_T) $= 10^4$ kN. Two dimensionless rotating velocities, $\bar{\Omega} = \Omega r_o \sqrt{\rho/E} = 0.15$ and 0.3, are studied. Convergence studies are carried out for both analytical method and MEM. As the analytical method involves Fourier series, its accuracy depends on the number of terms considered. For the model tested, 100 terms are found to be adequate in providing convergence in results for $r/r_o \leqslant 0.9$. The MEM involves the discretisation of the domain into a number of moving elements and its accuracy depends on the element mesh.

In studying the RD-SL problem, a uniform mesh of 15 bands and 24 sectors for MEM is used. Fig. 3 demonstrates the displacement and stress results for disk rotating at two different velocities with normal point load applied at the outer radius, whereas the solution for tangential point load is shown in Fig. 4. In general, the analytical and MEM solutions are found to be in good agreement. As the rotating velocity increases, the centrifugal effect becomes more dominating and the response in the radial direction approaches that for a freely rotating disk. The deviation between the analytical and MEM solutions at high velocities is due to the (erroneous) omission of $u_r\Omega^2$ term in the analytical solution.

A set of results in the SD-RL problem is also obtained, as shown in Fig. 5. As explained earlier, the SD-RL problem is readily solved by suppressing the Coriolis and centrifugal terms in the RD-SL solution. The results between the MEM and analytical solution are found to agree well.

A mesh of non-uniform elements can be generated such that refined elements are used where higher accuracy is required or where the solution varies sharply, e.g. in the vicinity of load point. However, since the load moves relative to finite elements, the load point would be outside the refined region if the FEM is used unless using re-meshing is carried out to follow the load location. Alternatively, if re-meshing is to be avoided, uniformly fine mesh has to be used for the whole disk. In contrast, the proposed MEM does not require re-mashing since the imaginary mesh is always fixed in relation to the load point. Furthermore, with non-uniform mesh, we can easily adjust the size of refined mesh to study the case of patch loading. To study uniform patch load over $-10^\circ \leqslant \alpha \leqslant 10^\circ$, a 15×24 mesh comprised of two different elements with 5° and 35°, as shown in Fig. 6, is used. The MEM results are in good agreement with the analytical solution as shown in Fig. 7.

The major difference between the RD-SL and SD-RL problems is associated with the centrifugal effect. In the RD-SL problem, the contributions by $u_r\Omega^2$ and the Coriolis term, $2\Omega^2\partial u_\eta/\partial\eta$, are overwhelmed by the centrifugal term $r\Omega^2$ in the radial direction. For rotating disk subjected to tangential point load, there is significant difference in response between RD-SL and SD-RL particularly when the rotating velocity is high. Fig. 8(a) shows that the shear stress response of rotating annular disk with $r_i/r_o = 0.3$ for RD-SL is much larger than for SD-RL at $\bar{\Omega} = 0.5$. However, the difference is very small for disk with higher radius ratio ($r_i/r_o = 0.5$) rotating at the same velocity as shown in Fig. 8(b). The difference is attributed to the presence of Coriolis term and $u_\eta\Omega^2$ term, which are present in the RD-SL case but not in the SD-RL case. The $u_\eta\Omega^2$ term is found to be the main contributor to the difference. This can be shown through the case of rotating disk subjected to uniform tangential load all round, for which the response of the disk is axisymmetrical and the Coriolis effect is absent.

Fig. 9 shows the circumferential displacements for disk with different radii ratios rotating under uniform tangential load applied along the outer boundary. It can be observed that at $\bar{\Omega} = 0.5$, the circumferential displacement for disk with $r_i/r_o = 0.3$ has increased greatly while there is little change for disk with larger radius ratio $r_i/r_o = 0.5$. The notation (m,n) denotes the critical mode with m oscillations in the radial direction and n oscillations in the circumferential direction. Fig. 9 also shows that for a sufficiently high rotating

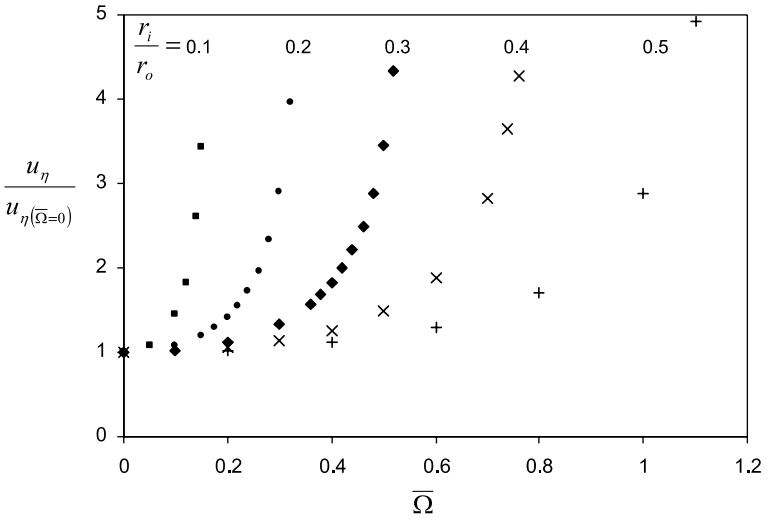

Fig. 9. Circumferential displacement for rotating disks of different radius ratios subjected to uniform tangential load.

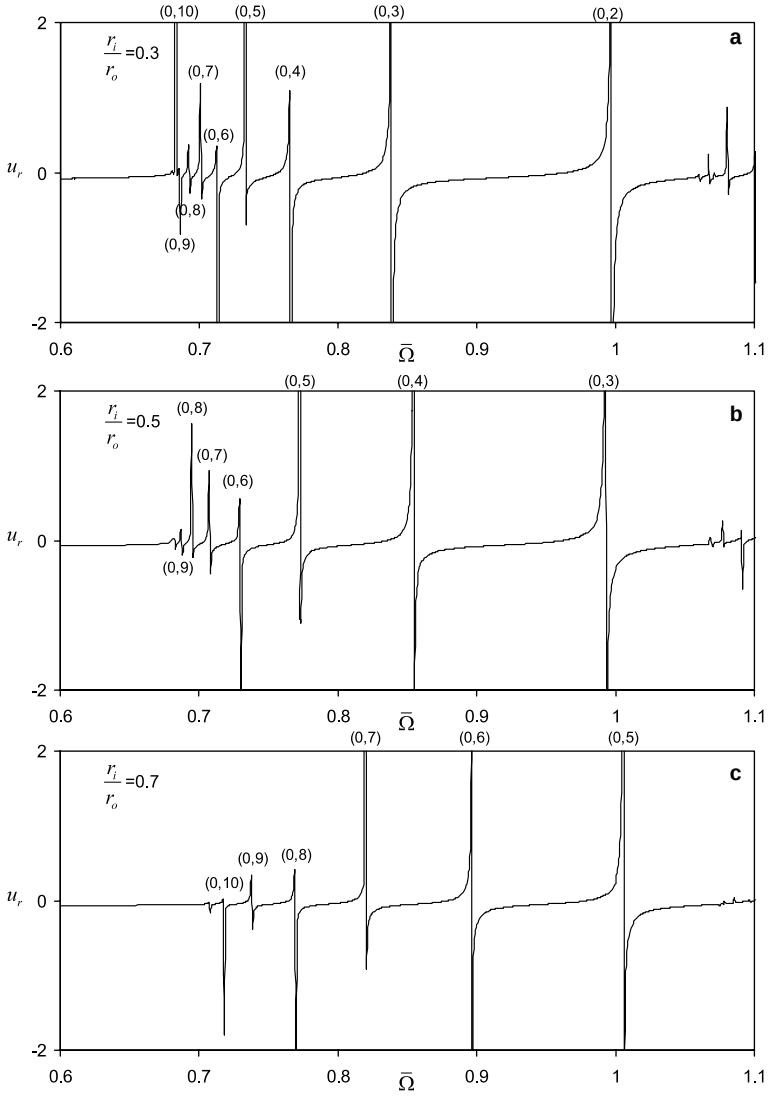

Fig. 10. Radial displacement, with displacement due to centrifugal effect removed, for rotating disks of different radius ratios subjected to normal point load.

velocity, the circumferential displacement becomes unbounded. The velocity when it happens depends on the radius ratio of the annular disk. This is the critical velocity for the fundamental mode $(0,0)$. To obtain the critical mode for $(0,n)$, the disk is subjected to normal point load and set to rotate at very high velocity. Fig. 10 shows the radial displacements, with displacement due to centrifugal effect removed, for annular disks with three different radius ratios $r_i/r_o = 0.3$, 0.5 and 0.7. With a 15×24 mesh, the highest mode observed is $(0,10)$. To observe an even higher mode, a finer mesh is required. It is observed that irregularity occurs when the rotating velocity is between 0.68 and 0.7. When the rotating velocity is increased further, the mode number decreases. Annular disk with smaller radius ratio ($r_i/r_o = 0.3$) would have the mode number decrease faster than that of larger radius ratio ($r_i/r_o = 0.7$). We can deduce that as the rotating velocity of annular disk increases, regardless of its radius ratio, it would first reach a critical velocity of the highest

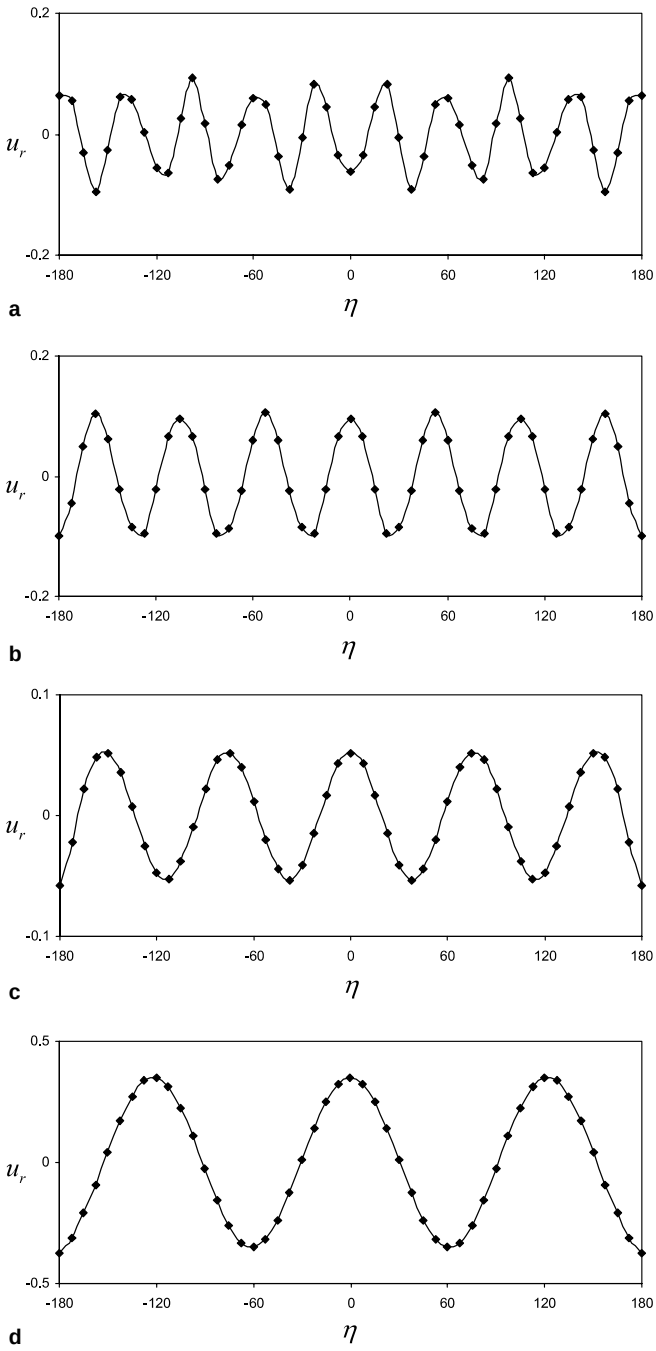

Fig. 11. Radial displacement, with displacement due to centrifugal effect removed, at different modes for annular disk with radius ratio 0.5, (a) mode $(0,9)$ at $\bar{\Omega} = 0.69$; (b) mode $(0,7)$ at $\bar{\Omega} = 0.71$; (c) mode $(0,5)$ at $\bar{\Omega} = 0.77$; (d) mode $(0,3)$ at $\bar{\Omega} = 1.00$.

mode. This agrees with the asymptotic critical velocity observed by Chen and Jhu (1997). Fig. 11 shows examples of various modes at their respective rotating velocities for radius ratio $r_i/r_o = 0.5$.

5. Conclusions

Both problems of RD-SL and SD-RL are studied both numerically and analytically. Analytical solutions are made more compact by using complex Fourier–Hankel series. Numerically, a new method is formulated which may be deemed as a paradigm shift. Though the problems considered are in the domain of solid mechanics (not fluid dynamics), the proposed moving elements are allowed to "flow" through the disk instead of being physically attached to the disk. The MEM presents a unified framework for solving both the RD-SL and SD-RL problems, the latter being treated as a special case of the former. The method can be extended to study out-of-plane response of rotating disks and other similar moving load problems.

As compared to the analytical solution, the MEM has the following advantages:

(a) In order to obtain analytical solution, it is necessary to ignore $u_r\Omega^2$ term in the RD-SL formulation. In the MEM, all terms are included.
(b) In cases of inclined loading, it is necessary for the analytical method to separate the problem into purely normal and purely tangential components. In the MEM, all loadings can be handled at the same time.
(c) The analytical method assumes uniform thickness throughout the disk. As a numerical method, the MEM is more versatile than the analytical method. For example, the applied load can be time-dependent for the MEM but not for the analytical method. The annular disk can also have different thickness values along the radial direction. These cases will be considered in future study.

As compared to the FEM, the MEM has the following advantages:

(a) In the FEM, it is necessary to keep track of the loading location (with respect to the elements and nodes) and to update the load vector at each step even if the applied load is constant. This problem does not exist in the MEM.
(b) In the MEM, the steady state response is obtained efficiently by solving an equivalent static problem.
(c) To enhance computational efficiency, it is advantageous to use non-uniform mesh such that finer elements are used, for instance, in the vicinity of load concentration where rapid change of stress is expected. Unlike the FEM, the MEM facilitates the easy use of non-uniform mesh which remains unchanged with respect to the load location.

Appendix A

A Fourier–Hankel solution is formulated based on Srinivasan and Ramamurti (1980). The following expressions demonstrate the case of SD-RL when the load is normal.

$$
\begin{aligned}
u_r = \sum_{n=1}^{\infty} \exp(\mathrm{i}n\eta)\Big\{ & c_n\Big[-\frac{n}{r}H_n^{(1)}(\alpha_1 n\Omega r) + \alpha_1 n\Omega H_{n-1}^{(1)}(\alpha_1 n\Omega r)\Big] + d_n\Big[\frac{n}{r}H_n^{(1)}(\alpha_2 n\Omega r)\Big] \\
& + e_n\Big[-\frac{n}{r}H_n^{(2)}(\alpha_1 n\Omega r) + \alpha_1 n\Omega H_{n-1}^{(2)}(\alpha_1 n\Omega r)\Big] + f_n\Big[\frac{n}{r}H_n^{(2)}(\alpha_2 n\Omega r)\Big]\Big\} \\
u_\eta = \sum_{n=1}^{\infty} -\mathrm{i}\exp(\mathrm{i}n\eta)\Big\{ & c_n\Big[\frac{n}{r}H_n^{(1)}(\alpha_1 n\Omega r)\Big] + d_n\Big[\frac{n}{r}H_n^{(1)}(\alpha_2 n\Omega r) - \alpha_2 n\Omega H_{n-1}^{(1)}(\alpha_2 n\Omega r)\Big] \\
& + e_n\Big[\frac{n}{r}H_n^{(2)}(\alpha_1 n\Omega r)\Big] + f_n\Big[\frac{n}{r}H_n^{(2)}(\alpha_2 n\Omega r) - \alpha_2 n\Omega H_{n-1}^{(2)}(\alpha_2 n\Omega r)\Big]\Big\}
\end{aligned}
$$

$$\sigma_{rr} = \sum_{n=1}^{\infty} \exp(\mathrm{i}n\eta)\Big\{ c_n \frac{2\mu}{r^2}[(n^2+n-0.5\alpha_2^2 n^2\Omega^2 r^2)H_n^{(1)}(\alpha_1 n\Omega r) - \alpha_1 n\Omega r H_{n-1}^{(1)}(\alpha_1 n\Omega r)]$$
$$+ d_n \frac{2\mu}{r^2}[(-n^2-n)H_n^{(1)}(\alpha_2 n\Omega r) + \alpha_2 n\Omega r H_{n-1}^{(1)}(\alpha_2 n\Omega r)]$$
$$+ e_n \frac{2\mu}{r^2}[(n^2+n-0.5\alpha_2^2 n^2\Omega^2 r^2)H_n^{(2)}(\alpha_1 n\Omega r) - \alpha_1 n\Omega r H_{n-1}^{(2)}(\alpha_1 n\Omega r)]$$
$$+ f_n \frac{2\mu}{r^2}[(-n^2-n)H_n^{(2)}(\alpha_2 n\Omega r) + \alpha_2 n\Omega r H_{n-1}^{(2)}(\alpha_2 n\Omega r)]\Big\}$$

$$\tau_{r\eta} = \sum_{n=0}^{\infty} -\exp(\mathrm{i}n\eta)\Big\{ c_n \frac{2\mu}{r^2}[(-n^2-n)H_n^{(1)}(\alpha_1 n\Omega r) + \alpha_1 n^2\Omega r H_{n-1}^{(1)}(\alpha_1 n\Omega r)]$$
$$+ d_n \frac{2\mu}{r^2}[(n^2+n-0.5\alpha_2^2 n^2\Omega^2 r^2)H_n^{(1)}(\alpha_2 n\Omega r) - \alpha_2 n\Omega r H_{n-1}^{(1)}(\alpha_2 n\Omega r)]$$
$$+ e_n \frac{2\mu}{r^2}[(-n^2-n)H_n^{(2)}(\alpha_1 n\Omega r) + \alpha_1 n^2\Omega r H_{n-1}^{(2)}(\alpha_1 n\Omega r)]$$
$$+ f_n \frac{2\mu}{r^2}[(n^2+n-0.5\alpha_2^2 n^2\Omega^2 r^2)H_n^{(2)}(\alpha_2 n\Omega r) - \alpha_2 n\Omega r H_{n-1}^{(2)}(\alpha_2 n\Omega r)]\Big\}$$

$$\sigma_{\eta\eta} = \sum_{n=1}^{\infty} \exp(\mathrm{i}n\eta)\Big\{ c_n \frac{2\mu}{r^2}\Big[\Big(-n^2-n-\frac{v}{1-v}\alpha_1^2 n^2\Omega^2 r^2\Big)H_n^{(1)}(\alpha_1 n\Omega r) + \alpha_1 n\Omega r H_{n-1}^{(1)}(\alpha_1 n\Omega r)\Big]$$
$$+ d_n \frac{2\mu}{r^2}[(n^2+n)H_n^{(1)}(\alpha_2 n\Omega r) - \alpha_2 n^2\Omega r H_{n-1}^{(1)}(\alpha_2 n\Omega r)]$$
$$+ e_n \frac{2\mu}{r^2}[(-n^2-n-\frac{v}{1-v}\alpha_1^2 n^2\Omega^2 r^2)H_n^{(2)}(\alpha_1 n\Omega r) + \alpha_1 n\Omega r H_{n-1}^{(2)}(\alpha_1 n\Omega r)]$$
$$+ f_n \frac{2\mu}{r^2}[(n^2+n)H_n^{(2)}(\alpha_2 n\Omega r) - \alpha_2 n^2\Omega r H_{n-1}^{(2)}(\alpha_2 n\Omega r)]\Big\}$$

where $\alpha_1^2 = \frac{\rho}{\lambda+2\mu}$, $\alpha_2^2 = \frac{\rho}{\mu}$ and $\lambda = \frac{Ev}{1-v^2}$, $\mu = \frac{E}{2(1+v)}$.

The solution has to be combined with that for $n = 0$, which corresponds to the case of disk subjected to uniform load at the outer boundary.

References

Chen, J.S., Jhu, J.L., 1997. In-plane stress and displacement distributions in a spinning annular disk under stationary edge loads. Journal of Applied Mechanics 64, 897–904.

Keith, M., Robert, N.M., 1981. Moving finite elements. SIAM Journal of Numerical Analysis 18, 1019–1032.

Koh, C.G., Ong, J.S.Y., Chua, D.K.H., Feng, J., 2003. Moving element method for train-track dynamics. International Journal for Numerical Methods in Engineering 56, 1549–1567.

Oden, J.T., Lin, T.L., 1986. On the general rolling contact problem for finite deformations of a viscoelastic cylinder. Computer Methods in Applied Mechanics and Engineering 57, 297–367.

Olsson, M., 1991. On the fundamental moving load problem. Journal of Sound and Vibration 145, 299–307.

Ougang, H., Mottershead, J.E., Li, W., 2003. A moving-load model for disc-brake stability analysis. Journal of Vibration and Acoustics 125, 53–58.

Srinivasan, V., Ramamurti, V., 1979. Analysis of an annular disc with a concentrated, in-plane edge load. Journal of Strain Analysis 14, 119–132.

Srinivasan, V., Ramamurti, V., 1980. Dynamic response of an annular disk to a moving concentrate, in-plane edge load. Journal of Sound and Vibration 72, 251–262.

Timoshenko, S.P., Goodier, J.N., 1982. Theory of Elasticity, third ed. McGraw-Hill, New York.